Capacitance of two-dimensional titanium carbide (MXene) and MXene/carbon nanotube composites in organic electrolytes

Yohan Dall'agnese, Patrick Rozier, Pierre-Louis Taberna, Yury Gogotsi, Patrice Simon

Capacitance of two-dimensional titanium carbide (MXene) and MXene/carbon nanotube composites in organic electrolytes

Yohan Dall'Agnese [a, b, c], Patrick Rozier [a, b], Pierre-Louis Taberna [a, b], Yury Gogotsi [c], Patrice Simon [a, b, *]

[a] Université Paul Sabatier, CIRIMAT UMR CNRS 5085, 118 Route de Narbonne, 31062 Toulouse, France
[b] Réseau sur le Stockage Electrochimique de l'Energie (RS2E), FR CNRS 3459, France
[c] Department of Materials Science and Engineering, A. J. Drexel Nanomaterials Institute, Drexel University, Philadelphia, PA 19104, USA

HIGHLIGHTS

- 3 types of Ti_3C_2 electrodes were prepared: clay, delaminated and CNT composite.
- Capacitance up to 245 F cm^{-3} in 1 M EMITFSI solution in acetonitrile was achieved.
- Imidazolium (EMI^+) ions intercalation was demonstrated by *in situ* XRD.

GRAPHICAL ABSTRACT

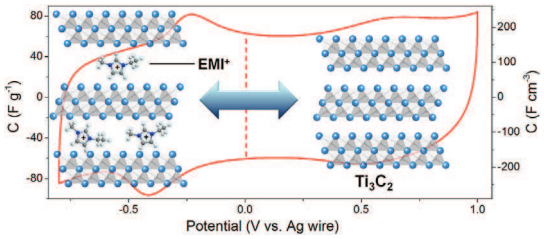

ABSTRACT

Pseudocapacitive materials that store charges by fast redox reactions are promising candidates for designing high energy density electrochemical capacitors. MXenes – recently discovered two-dimensional carbides, have shown excellent capacitance in aqueous electrolytes, but in a narrow potential window, which limits both the energy and power density. Here, we investigated the electrochemical behavior of Ti_3C_2 MXene in 1M solution of 1-ethly-3-methylimidazolium bis-(trifluoromethylsulfonyl)-imide (EMITFSI) in acetonitrile and two other common organic electrolytes. This paper describes the use of clay, delaminated and composite Ti_3C_2 electrodes with carbon nanotubes in order to understand the effect of the electrode architecture and composition on the electrochemical performance. Capacitance values of 85 F g^{-1} and 245 F cm^{-3} were obtained at 2 mV s^{-1}, with a high rate capability and good cyclability. *In situ* X-ray diffraction study reveals the intercalation of large EMI^+ cations into MXene, which leads to increased capacitance, but may also be the rate limiting factor that determines the device performance.

Keywords:
Electrochemical capacitors
Two-dimensional materials
MXene
X-ray diffraction
Carbon nanotube, titanium carbide

1. Introduction

Electrochemical capacitors (ECs) are commercial devices used for high power delivery applications [1,2]. They typically utilize either porous carbon materials or pseudocapacitive materials for electrostatic or redox energy storage, respectively [3,4]. In the latter, the charge is stored by fast redox reactions at the surface of materials such as MnO_2, RuO_2, Nb_2O_5 or MoO_3 [5–8]. Recently, energy storage based on ion intercalation into two-dimensional (2D) materials has attracted much attention because of promising results with up to 375 F g^{-1} in KOH or 200 F g^{-1} in organic electrolyte for functionalized graphene [9,10].

* Corresponding author. Université Paul Sabatier, CIRIMAT UMR CNRS 5085, 118 route de Narbonne, 31062 Toulouse, France.
E-mail address: simon@chimie.ups-tlse.fr (P. Simon).

http://dx.doi.org/10.1016/j.jpowsour.2015.12.036

A new family of two-dimensional materials called MXenes has emerged as promising electrodes for energy storage devices such as batteries [11–15], metal ion (Li^+, Na^+) capacitors [16–18] and ECs [19–22]. MXenes are synthetized by selective etching of the A layer from the conductive ternary carbide family of MAX phases [23]. Of the MXene family, Ti_3C_2 was the first discovered and is the most studied to date. First studies of Ti_3C_2 as electrode material in supercapacitors showed capacities up to 100 F g^{-1} for intercalation of cations such as Li^+, Mg^{2+} or Al^{3+} in aqueous electrolytes [19]. Aside, MXene performance can be greatly improved by tuning the surface functional groups, delamination or addition of carbon nanoparticles [14,21,22]. Delaminated Ti_3C_2 electrodes containing carbon nanotubes have also shown noteworthy performance in lithium ion batteries, as well as in aqueous supercapacitors with capacity up to 430 mAh g^{-1} and capacitance of 140 F g^{-1}, respectively [14,22]. The modification of the chemistry of the surface groups through a new "clay" synthesis route led to a 2-fold increase in volumetric capacitance (up to 900 F cm^{-3}) in sulfuric acid electrolyte due to dense packing of 2D MXene sheets combined with their accessibility due to pre-intercalation of ions during the synthesis [20]. The role of pseudocapacitance in these high values was confirmed by showing a reversible change in the oxidation state of titanium atoms in MXene [24].

However, MXene has been investigated as electrode material for ECs mainly in aqueous electrolytes, which show a limited potential window due to water electrolysis. Moreover, oxidation of Ti_3C_2 under high anodic potentials in aqueous electrolytes further limits its use to cathodes of asymmetric devices. As both the energy and the power density increase with the square of the potential window, its expansion is one of the key challenges for designing SCs with improved performance and organic electrolyte may expand the voltage window beyond 2–2.5 V.

In this work, we report on the electrochemical performance of Ti_3C_2 in organic supercapacitor electrolytes for supercapacitor applications. The energy storage mechanism was studied by *in situ* X-ray diffraction (XRD).

2. Experimental

2.1. Electrode preparation

Ti_3C_2 was synthesized by selectively etching the aluminum layer out of the Ti_3AlC_2 MAX phase in a 6M HCl/LiF solution at 35 °C for 24 h [20]. The obtained material was then washed with distilled water. MXene samples after synthesis were terminated with OH, O and F and we add T_x to the Ti_3C_2 formula to show those surface terminations. Full delamination of $Ti_3C_2T_x$ was obtained by ultrasonication for 1 h in distilled water. A composite material was prepared by mixing the colloidal solution of delaminated Ti_3C_2 with 20 wt. % of multiwalled carbon nanotubes (MWCNT C100, Graphistrength) which have specific surface area of 175 m^2 g^{-1}. The as-synthetized $Ti_3C_2T_x$, the delaminated $Ti_3C_2T_x$ and the CNT/$Ti_3C_2T_x$ composite were filtered on polypropylene membranes then rolled into film electrodes on Teflon membranes using a glass tube. Once dried, the films were easily removed from the membrane to obtain the freestanding $Ti_3C_2T_x$, d-$Ti_3C_2T_x$ and CNT-$Ti_3C_2T_x$ films without binder. The electrodes were prepared by cutting the films into ~25 mm^2 rectangles with a razor blade. The thicknesses were measured from scanning electron microscope observations and $Ti_3C_2T_x$, d-$Ti_3C_2T_x$ and CNT-$Ti_3C_2T_x$ film densities were calculated to be 2.3 g cm^{-3}, 3.0 g cm^{-3} and 2.9 g cm^{-3}, respectively.

2.2. Electrochemical testing

Three-electrode Swagelok© cells were used with Ti_3C_2 as working electrode, an Ag wire as a pseudo-reference electrode and a commercial activated carbon (YP17 Kuraray, Japan) overcapacitive counter electrode prepared by mixing 5 wt.% polytetrafluoroethylene binder (60 wt.% in H_2O, Aldrich) to 95 wt.% of YP17. A polypropylene membrane (GH Polypro, Pall) was used as a separator. The electrolyte was a 1 M solution of EMITFSI (1-ethyl-3-methylimidazolium bis(trifluoromethylsulfonyl)imide, Solvionic) in acetonitrile (Acros Organics). For comparison purposes, 1 M $EMIBF_4$ (1-ethyl-3-methylimidazolium tetrafluoroborate, Fluka) and 1 M $TEABF_4$ (tetraethylammonium tetrafluoroborate, Acros Organics) in acetonitrile were tested. The cells were assembled in an argon-filled glovebox. A VMP3 potentiostat (Biologic SA, France) was used for electrochemical testing. Cyclic voltammetry (CV) was performed at scan rates from 2 to 100 mV s^{-1}; capacitance values were calculated by integrating the reduction current. Galvanostatic charge–discharge measurements were performed at 1 A g^{-1} and corresponding capacitances were calculated from the slopes of the curves. Gravimetric capacitances were calculated from the total mass of the composite electrode; associated volumetric capacitances were obtained using the density of the respective electrodes. Electrochemical impedance spectroscopy (EIS) was performed between 100 mHz and 200 kHz in two-electrode configuration after polarization at 0.5 V *vs.* Ag using a three-electrode setup.

2.3. Material characterization

A scanning electron microscope (SEM, JSM-6700F, JEOL) was used to investigate the electrodes' morphology and structure. X-ray diffraction (XRD) patterns of the CNT-Ti_3C_2 electrodes were collected by a Brucker D8 diffractometer using a Cu K_α radiation ($\lambda = 1.5406$ Å) in the range $2\theta = 5–50°$ with a step of 0.016°. The samples were polarized at different potentials using a 2-electrode cell (LRCS, University de Picardie Jules Verne, Amiens, France) covered with a beryllium window served as the current collector, avoiding electrolyte evaporation and allowing *in situ* electrochemical XRD. Nitrogen sorption analysis at 77 K using Micromeritics ASAP 2020 apparatus was carried out for calculating the specific surface area (SSA) using the Brunauer–Emmet–Teller (BET) equation after outgassing under vacuum at 300 °C for 12 h.

3. Results and discussion

Fig. 1 shows cross-section SEM images of electrode materials. The as-prepared MXene clay, denoted as $Ti_3C_2T_X$, is shown in Fig. 1a. MXene layers can be rolled and sheared, forming a freestanding flexible electrode [20,21]. Fully delaminated MXene electrodes, denoted as d-$Ti_3C_2T_X$ (Fig. 1b), were prepared for improving the electrochemical performance by taking advantage of a higher specific surface area (SSA) resulting from delamination. The SSA values were 23 m^2 g^{-1} for multilayered Ti_3C_2 and 98 m^2 g^{-1} for delaminated Ti_3C_2 measured elsewhere by nitrogen gas sorption analysis [12]. However, previous studies demonstrated that restacking of delaminated MXene layers forming a dense MXene "paper" with in-plane alignment of MXene sheets limits the accessibility of electrolyte ions. Such restacking issue can be prevented by addition of carbon nanoparticles [14,22]. Accordingly, composite electrodes were prepared by mixing appropriate amounts of d-$Ti_3C_2T_X$ and MWCNTs. The SSA obtained by nitrogen gas sorption analysis was 70 m^2 g^{-1} for the CNT-$Ti_3C_2T_X$. Fig. 1c–d shows SEM images of a cross-section of the CNT-$Ti_3C_2T_X$ composite electrode, where CNTs are homogeneously spread between the Ti_3C_2 layers since no aggregates can be seen. Aside preventing restacking, CNT addition is known to increase the conductivity of the electrodes [14,22,25–27].

Fig. 2 shows cyclic voltammograms (CVs) of the three Ti_3C_2-

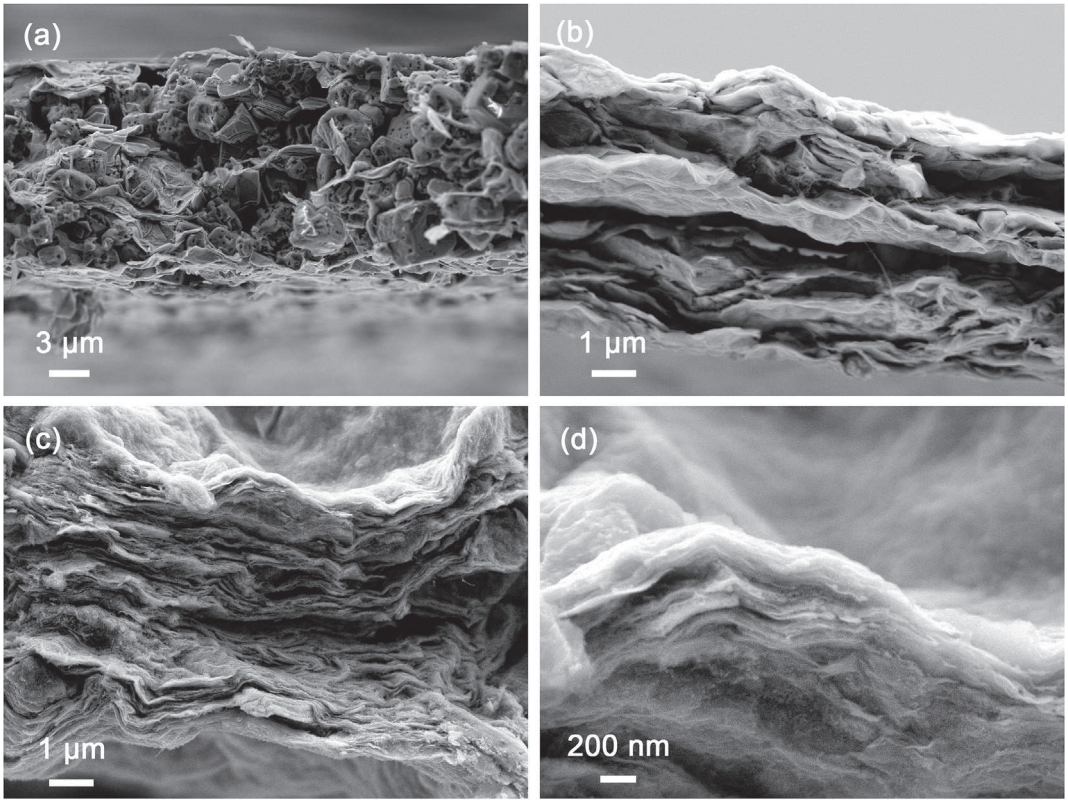

Fig. 1. Scanning electron microscope images of (a) rolled $Ti_3C_2T_X$ "clay", (b) d-$Ti_3C_2T_X$ and (c–d) CNT-$Ti_3C_2T_X$ electrode films.

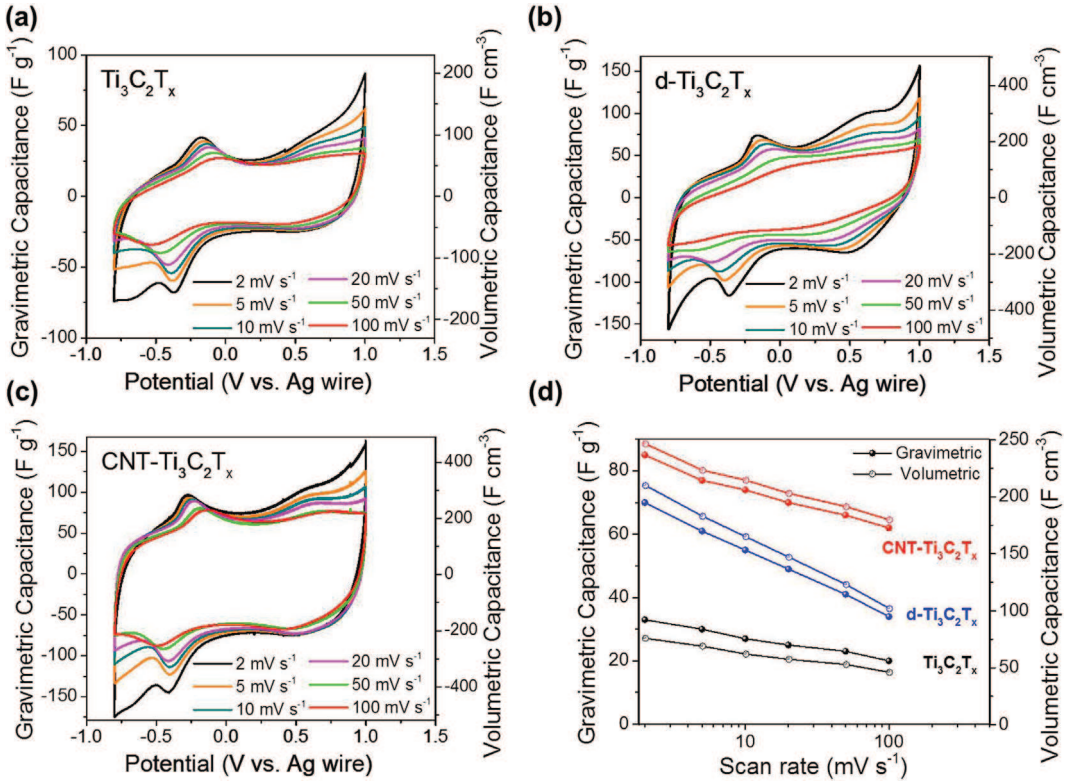

Fig. 2. Cyclic voltammograms of (a) $Ti_3C_2T_x$, (b) d-$Ti_3C_2T_x$ and (c) CNT-$Ti_3C_2T_x$ in 1M EMITFSI in acetonitrile electrolyte at different scan rates and (d) summary of the change of capacitance with the potential scan rate. These measurements were done using a three-electrode Swagelok cell.

based electrodes at 20 mV s^{-1} in 1M EMITFSI in acetonitrile. The electrochemical signatures of the three samples appear to be similar, characterized by a capacitive envelope and a set of redox peaks around −0.2 V and −0.4 V *vs.* Ag. The potential difference between the oxidation and the reduction peaks, associated with kinetics and ohmic limitations, changes from one electrode to another. The smaller difference is observed for CNT-$Ti_3C_2T_x$ that can be associated in a first approach to a faster diffusion path, thanks to the addition of CNTs. $Ti_3C_2T_x$ shows similar electrochemical signature with a slightly larger overpotential and d-$Ti_3C_2T_x$ shows the largest overpotential and more resistive behavior, possibly due to the restacking of delaminated layers during electrode preparation. The potential range (1.8 V) is narrower than expected from this electrolyte, but could be explained by water trapped between Ti_3C_2 layers, responsible for electrolyte reaction at the extrema of the potential range visible at low scan rates.

The change of the capacitance (calculated from the integration of the charge during CV measurements) with the potential scan rate is shown Fig. 2d. Capacitance up to 245 F cm^{-3} (85 F g^{-1}) was obtained at 2 mV s^{-1} for CNT-Ti_3C_2, with 75% capacitance retention at 100 mV s^{-1} (50% for d-$Ti_3C_2T_x$). This performance highlights a fairly high power capability of the electrodes, which is assumed to originate from the open 2D structure of the material and the associated high accessibility of the surface to ions. The lower rate performance of d-Ti_3C_2 could be attributed to poor charge percolation.

The electrochemical impedance spectroscopy measurements (Fig. 3) on the three different samples at a bias voltage of 0.5 V (OCV) suggest that the addition of MWCNT greatly improves the charge percolation of the electrode. Additionally, there is little to no influence of MWCNTs on the electronic conductivity of the electrode, as can be seen from the constant value of the high-frequency resistance. This can be explained by a much higher conductivity of metallic $Ti_3C_2T_x$ electrode films (~2000 S cm^{-1} [28]) compared to conventional activated carbon, oxide or even graphene electrodes.

Fig. 4a–c shows the galvanostatic charge–discharge curves obtained at 1A g^{-1} of the three electrodes. The curves are almost linear but contain a slight change in their slopes which correspond to the redox peaks identified previously. It appears that the electrodes exhibit pseudo-capacitive behavior. Also, a 5–10 times lower specific surface area of MXene [19] compared to activated carbons [4] would lead to a very low capacitance without contribution of charge-transfer processes. Fig. 4d shows the cycle life for the different electrodes, at 1A g^{-1}. CNT-$Ti_3C_2T_x$ shows a good stability, with 90% capacitance retention after 1000 cycles. $Ti_3C_2T_x$ and d-$Ti_3C_2T_x$ show a lower stability and faster capacitance decrease during cycling, as well as a lower coulombic efficiency.

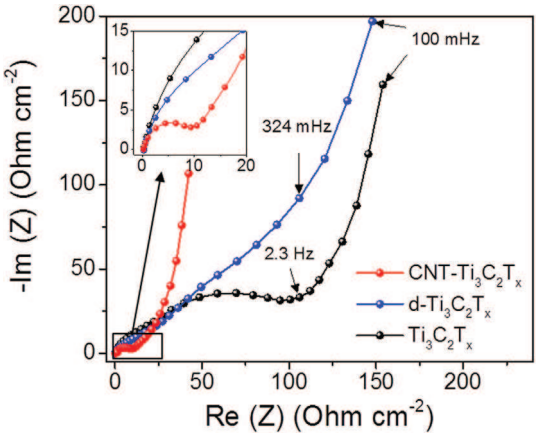

Fig. 3. Nyquist plot at 0.5 V *vs.* Ag reference obtained using a two-electrode setup.

The energy storage mechanism was investigated by recording *in situ* XRD patterns at different potentials (Fig. 5a). The comparison of patterns indicates that depending on the applied potential two different sets of Bragg peaks are observed and that the phase change occurs at the same potential were the set of redox peaks appears in the CV (Fig. 2c). This shows that intercalation/deintercalation processes follow a reversible two-phase mechanism, which differs from the progressive and continuous intercalation process previously observed for MXenes materials in aqueous supercapacitor [19] and metal-ions capacitors [16,17]. Each set of Bragg peaks can be indexed, in agreement with *Ghidiu* et al. [20], using the (00l) diffraction planes of Ti_3C_2 which are characteristic of the interlayer space. On the basis of the diffraction angle of (002) Bragg peaks (Fig. 5b), it can be deduced that in the −0.8 V to −0.5 V potential range, the interlayer distance is 1.3 Å larger than at potentials above −0.5 V and should correspond to the intercalation and de-intercalation of ions from the electrolyte into $Ti_3C_2T_x$.

Considering the low value of the intercalation potential, one can assume in a first approximation that the expansion is due to the intercalation of the EMI^+ cations between Ti_3C_2 layers and the shrinkage is attributed to its de-intercalation. Reversible intercalation of organic ions accompanied by peaks in CVs was observed for porous carbon electrodes, when the ion size was somewhat larger than the pore size [29]. Interestingly when cycled within the 0.1 V–1 V potential range, $Ti_3C_2T_x$ capacitance quickly decreases with the cycle number, while it is more stable when cycled between −0.8 V and 0.1 V, as shown Fig. 6. This suggests that the capacitive behavior observed above 0 V is associated with a redox process at negative potentials. In other 2D materials, it is admitted that the intercalation of ions can form a pillared structure [18,30–32]. It is possible that cycling exclusively in the positive region causes the structure to collapse.

Further evidence that the redox reaction is due to the intercalation of cations is provided by comparison of the CVs of CNT-$Ti_3C_2T_x$ in 1M solutions of EMITFSI, $EMIBF_4$ and $TEABF_4$ in acetonitrile. Fig. 7a shows the CV of the CNT-$Ti_3C_2T_x$ electrode in 1 M $EMIBF_4$ in acetonitrile electrolyte (a smaller anion but the same cation as in Fig. 2). The electrochemical signature is similar to that obtained in 1M EMITFSI in acetonitrile electrolyte (Fig. 2); more specifically, we note the presence of a set of redox peaks at the same potential. Fig. 7b shows the CV of the CNT-$Ti_3C_2T_x$ electrode in 1 M $TEABF_4$ in acetonitrile electrolyte. When replacing the "planar" EMI^+ cation with the larger and more "spherical" TEA^+ cation, the electrochemical response is drastically changed. The reduction (intercalation) peak is present at a lower potential (−1 V vs Ag wire), but the reaction seems irreversible with an oxidation wave shifted to about 0.5 V. Probably, large TEA^+ ions are stuck between MXene sheets after intercalation, decreasing the reversibility of the process, but also contributing to pillaring. These measurements suggest that the intercalation/deintercalation of the EMI^+ cation is responsible for the reversible redox process occurring at −0.4 V *vs.* Ag. This hypothesis should be further confirmed by other *in situ* characterization techniques, such as electrochemical quartz crystal microbalance [33] or nuclear magnetic resonance [34].

4. Conclusions

The electrochemical behavior of $Ti_3C_2T_x$ as an electrochemical capacitor electrode in organic electrolytes has been investigated. Capacitance up to 32 F g^{-1} was obtained for as-produced $Ti_3C_2T_x$ MXene clay and improved to 85 F g^{-1} by delamination and addition of carbon nanotubes. Intercalation of large EMI^+ cations between the layers of Ti_3C_2 has been demonstrated suggesting that other large or multivalent cations may be similarly intercalated into

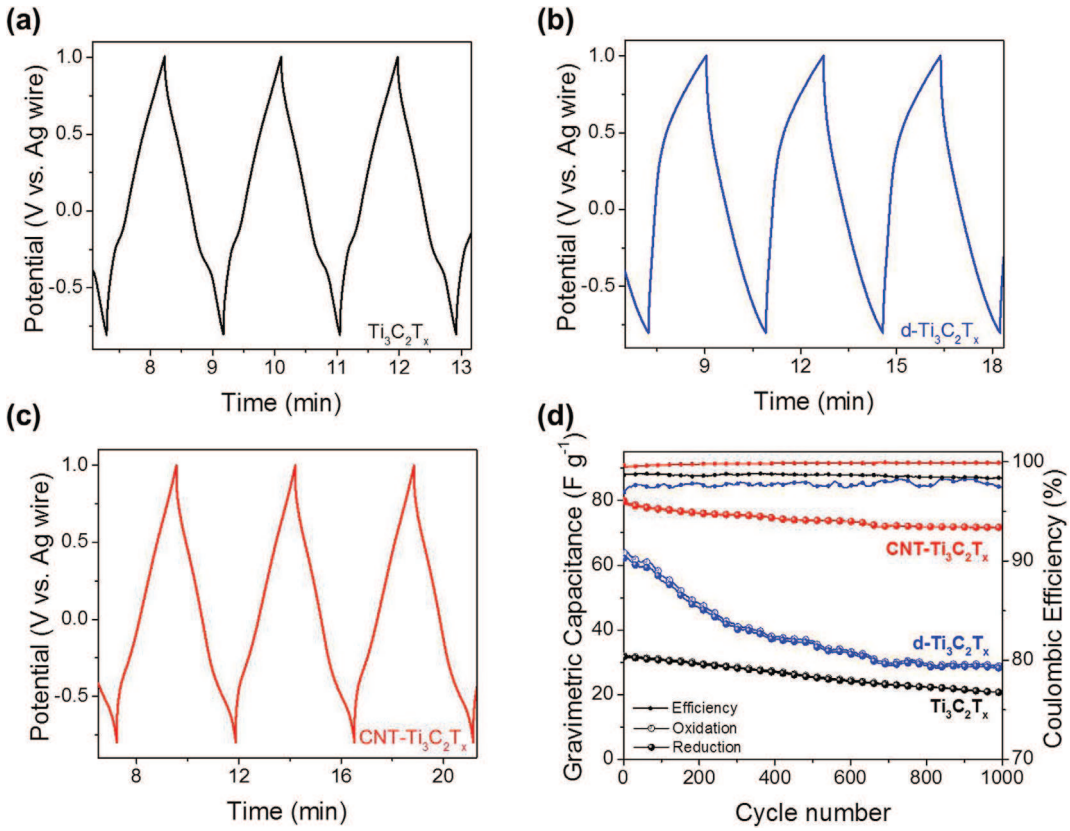

Fig. 4. Galvanostatic charge–discharge curves of (a) $Ti_3C_2T_x$, (b) d-$Ti_3C_2T_x$ and (c) CNT-$Ti_3C_2T_x$ in 1M EMITFSI in acetonitrile electrolyte obtained at 1 A g^{-1} and (d) the corresponding cycle life of those electrodes. These measurements were done using a three-electrode Swagelok cell.

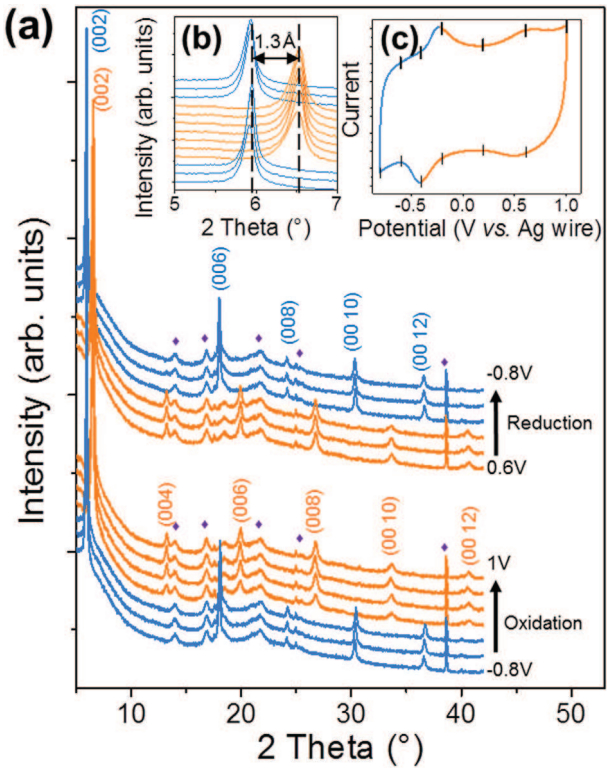

Fig. 5. In-situ XRD patterns of CNT-$Ti_3C_2T_x$ at different potentials in the 5–42° 2θ range. Purple diamonds indicate peaks coming from the cell for *in situ* measurements. Inset (b) shows a zoom in the 5–7° 2θ range and (c) CV recorded at 20 mV s^{-1}. (For interpretation of the references to color in this figure legend, the reader is referred to the web version of this article.)

MXenes from organic electrolyte solutions. $Ti_3C_2T_x$ capacitance was increased 3-fold, up to 85 F g^{-1} and 245 F cm^{-3} at 2 mV s^{-1} by using carbon nanotubes as an additive to improve ion accessibility to the active material. The CNT/$Ti_3C_2T_x$ electrodes show a good rate performance and good cycle life stability. Considering that this is the first report on capacitance of Ti_3C_2 in organic electrolytes used in supercapacitors and that Ti_3C_2 is only one of more than a dozen of already synthesized MXenes, there are good reasons to expect further improvement in capacitance as the optimal MXene-

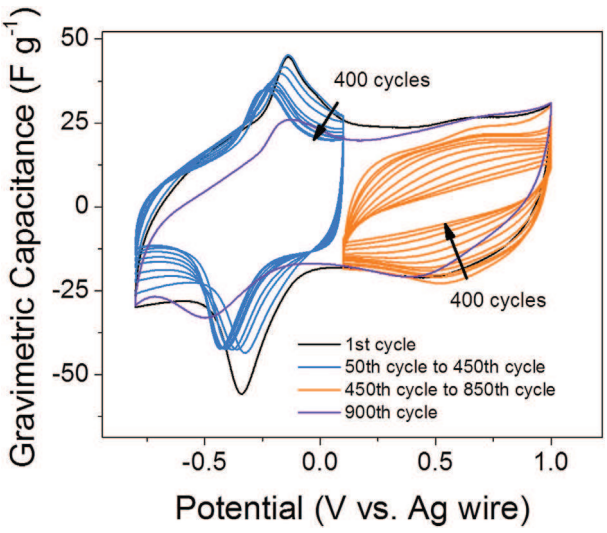

Fig. 6. Cyclic voltammograms of $Ti_3C_2T_x$ in different potential ranges at 20 mV s^{-1}.

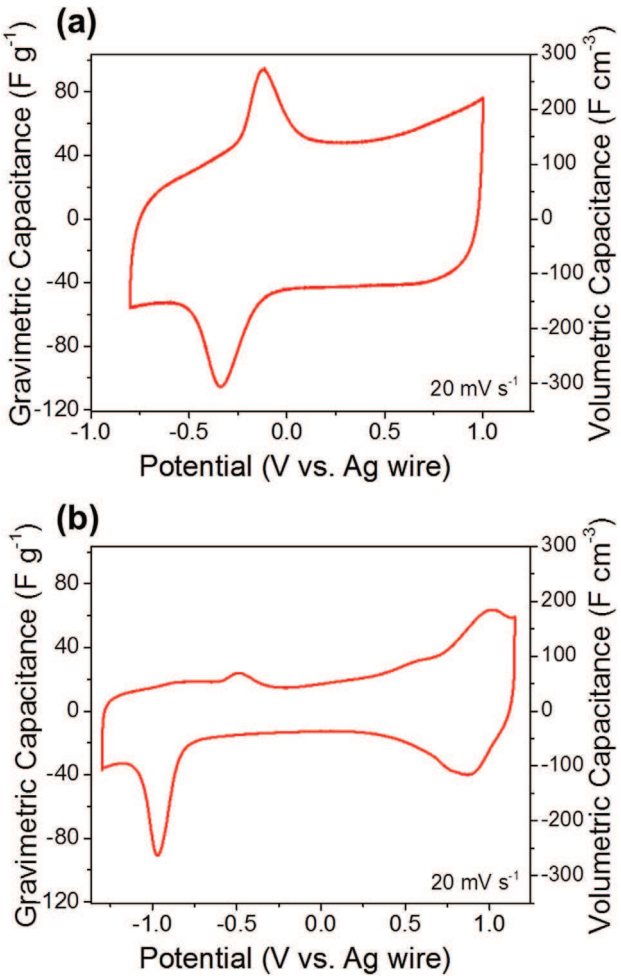

Fig. 7. Cyclic voltammetry of CNT-$Ti_3C_2T_x$ at 20 mV s^{-1} in 1 M solutions of $EMIBF_4$ (a) and $TEABF_4$ in acetonitrile (b).

electrolyte couples have been identified and their performance optimized. It took less than two years to increase capacitance of Ti_3C_2-MXene in aqueous electrolyte from about 100 F g^{-1} [19] to 320 F g^{-1} [21] and we expect fast improvement of capacitance in organic electrolytes as well.

Acknowledgment

We thank C. E. Ren for help with material synthesis, Kathleen Maleski for comments on the manuscript (both, Drexel University), B. Daffos for the SEM images and gas sorption analysis, and B. Duployer for help in *in situ* XRD experiments (both, Université Paul Sabatier). This work was supported by the Partnership Universities Fund (PUF) of French Embassy. YDA was supported by the European Research Council (ERC, Advanced Grant, ERC-2011-AdG, Project 291543 – IONACES). PS acknowledges the funding from the Chair of Excellence of the Airbus group foundation "Embedded multi-functional materials".

References

[1] M. Armand, J.M. Tarascon, Nature 451 (2008) 652–657.
[2] J.R. Miller, P. Simon, Science 321 (2008) 651–652.
[3] L.L. Zhang, X.S. Zhao, Chem. Soc. Rev. 38 (2009) 2520–2531.
[4] P. Simon, Y. Gogotsi, Nat. Mater. 7 (2008) 845–854.
[5] J.P. Zheng, P.J. Cygan, T.R. Jow, J. Electrochem. Soc. 142 (1995) 2699–2703.
[6] H.Y. Lee, J.B. Goodenough, J. Solid State Chem. 144 (1999) 220–223.
[7] V. Augustyn, P. Simon, B. Dunn, Energy Environ. Sci. 7 (2014) 1597–1614.
[8] X. Xiao, C. Zhang, S. Lin, L. Huang, Z. Hu, Y. Cheng, T. Li, W. Qiao, D. Long, Y. Huang, L. Mai, Y. Gogotsi, J. Zhou, Energy Storage Mater. 1 (2015) 1–8.
[9] Y. Zhu, S. Murali, M.D. Stoller, K.J. Ganesh, W. Cai, P.J. Ferreira, A. Pirkle, R.M. Wallace, K.A. Cychosz, M. Thommes, D. Su, E.A. Stach, R.S. Ruoff, Science 332 (2011) 1537–1541.
[10] Z. Fan, J. Yan, L. Zhi, Q. Zhang, T. Wei, J. Feng, M. Zhang, W. Qian, F. Wei, Adv. Mater. 22 (2010) 3723–3728.
[11] M. Naguib, J. Come, B. Dyatkin, V. Presser, P.-L. Taberna, P. Simon, M.W. Barsoum, Y. Gogotsi, Electrochem. Commun. 16 (2012) 61–64.
[12] O. Mashtalir, M. Naguib, V.N. Mochalin, Y. Dall'Agnese, M. Heon, M.W. Barsoum, Y. Gogotsi, Nat. Commun. 4 (2013) 1716.
[13] Y. Xie, Y. Dall'Agnese, M. Naguib, Y. Gogotsi, M.W. Barsoum, H.L. Zhuang, P.R.C. Kent, ACS Nano 8 (2014) 9606–9615.
[14] Y. Liu, W. Wang, Y. Ying, Y. Wang, X. Peng, Dalton Trans. 44 (2015) 7123–7126.
[15] M. Naguib, J. Halim, J. Lu, K.M. Cook, L. Hultman, Y. Gogotsi, M.W. Barsoum, J. Am. Chem. Soc. 135 (2013) 15966–15969.
[16] J. Come, M. Naguib, P. Rozier, M.W. Barsoum, Y. Gogotsi, P.L. Taberna, M. Morcrette, P. Simon, J. Electrochem. Soc. 159 (2012) A1368–A1373.
[17] Y. Dall'Agnese, P.-L. Taberna, Y. Gogotsi, P. Simon, J. Phys. Chem. Lett. 6 (2015) 2305–2309.
[18] X. Wang, S. Kajiyama, H. Iinuma, E. Hosono, S. Oro, I. Moriguchi, M. Okubo, A. Yamada, Nat. Commun. 6 (2015) 6544.
[19] M.R. Lukatskaya, O. Mashtalir, C.E. Ren, Y. Dall'Agnese, P. Rozier, P.L. Taberna, M. Naguib, P. Simon, M.W. Barsoum, Y. Gogotsi, Science 341 (2013) 1502–1505.
[20] M. Ghidiu, M.R. Lukatskaya, M.-Q. Zhao, Y. Gogotsi, M.W. Barsoum, Nature 516 (2014) 78–81.
[21] Y. Dall'Agnese, M.R. Lukatskaya, K.M. Cook, P.-L. Taberna, Y. Gogotsi, P. Simon, Electrochem. Commun. 48 (2014) 118–122.
[22] M.-Q. Zhao, C.E. Ren, Z. Ling, M.R. Lukatskaya, C. Zhang, K.L. Van Aken, M.W. Barsoum, Y. Gogotsi, Adv. Mater. 27 (2015) 339–345.
[23] M. Naguib, Y. Gogotsi, Acc. Chem. Res. 48 (2015) 128–135.
[24] M.R. Lukatskaya, S.-M. Bak, X. Yu, X.-Q. Yang, M.W. Barsoum, Y. Gogotsi, Adv. Energy Mater. 5 (2015) 1500589.
[25] Q. Cheng, J. Tang, J. Ma, H. Zhang, N. Shinya, L.-C. Qin, Phys. Chem. Chem. Phys. 13 (2011) 17615–17624.
[26] X.-M. Liu, Z.D. Huang, S.W. Oh, B. Zhang, P.-C. Ma, M.M.F. Yuen, J.-K. Kim, Compos. Sci. Technol. 72 (2012) 121–144.
[27] B.J. Landi, M.J. Ganter, C.D. Cress, R.A. DiLeo, R.P. Raffaelle, Energy & Environ. Sci. 2 (2009) 638–654.
[28] Z. Ling, C.E. Ren, M.-Q. Zhao, J. Yang, J.M. Giammarco, J. Qiu, M.W. Barsoum, Y. Gogotsi, Proc. Natl. Acad. Sci. 111 (2014) 16676–16681.
[29] R. Lin, P. Huang, J. Ségalini, C. Largeot, P.L. Taberna, J. Chmiola, Y. Gogotsi, P. Simon, Electrochim. Acta 54 (2009) 7025–7032.
[30] M.M. Hantel, R. Nesper, A. Wokaun, R. Kötz, Electrochim. Acta 134 (2014) 459–470.
[31] Y. Dong, X. Xu, S. Li, C. Han, K. Zhao, L. Zhang, C. Niu, Z. Huang, L. Mai, Nano Energy 15 (2015) 145–152.
[32] H. Li, G. Zhu, Z. Yang, Z. Wang, Z.-H. Liu, J. Colloid Interface Sci. 345 (2010) 228–233.
[33] M.D. Levi, M.R. Lukatskaya, S. Sigalov, M. Beidaghi, N. Shpigel, L. Daikhin, D. Aurbach, M.W. Barsoum, Y. Gogotsi, Adv. Energy Mater. 5 (2015) 1400815.
[34] J.M. Griffin, A.C. Forse, W.-Y. Tsai, P.-L. Taberna, P. Simon, C.P. Grey, Nat. Mater. 14 (2015) 812–819.